Optical spectroscopy of hydrogenic atoms

Tony Hyun Kim
MIT Department of Physics
(Dated: October 31, 2008)

We measure the Balmer lines of hydrogen and deuterium. The hydrogen Rydberg is computed, $R'_{H,ex} = (1.09678 \pm 0.00002) \times 10^7 \mathrm{m}^{-1}$, and is shown to be in remarkable agreement with the accepted value, $R_{NIST} = 1.096776 \times 10^7 \mathrm{m}^{-1}$. From the ratio of the Rydberg constants, we also obtain the $^1H/^2H$ mass ratio: $m_D/m_H = 1.86 \pm 0.16$. This is to be compared with the published value of $m_D/m_H = 1.999$. Finally, we provide a table of fine-structure splittings in sodium.

1. INTRODUCTION

We investigate the emission spectra of atoms containing a single optical electron. As early as the late 19th century, the *Rydberg formula* (Eq. 1) was empirically obtained, and was known to quantitatively predict the emission wavelengths λ by the rule:

$$\frac{1}{\lambda} = R\left(\frac{1}{n_i^2} - \frac{1}{n_f^2}\right) \tag{1}$$

where R is called the *Rydberg constant*, and n_i, n_f are positive integers such that $n_i > n_f$.

Our measurements verify the Rydberg formula for hydrogen and deuterium. Such observations have provided a crucial experimental basis for the development of quantum mechanics. In fact, it was mainly Bohr's derivation of R from fundamental constants that initially justified his radical notion of discrete atomic states. In this paper, we also use the ratio of the respective Rydberg constants to compute the $^1\mathrm{H}/^2\mathrm{H}$ mass ratio.

The subsequent Schrödinger theory provides a formalism for treating higher-order effects in the atom, beyond the Coulombic field that gives rise to Eq. 1. We observe the most significant of such effects in sodium, called the *fine-structure* splittings. The splitting is observed spectroscopically by the identification of "doublet" structures in the Na spectral lines.

2. THEORETICAL BACKGROUND

2.1. QM of the optical electron

The basic physics of atomic structure is the Coulombic interaction between the positively-charged nucleus and the optical electron. As usual, the two-body problem is simplified by the introduction of relative coordinates and the reduced mass μ. This results in a single-particle Schrödinger equation, yielding in the case of hydrogen ($Z = 1$) the following eigenenergies:

$$E_n = -\left[\frac{\mu}{2\hbar^2}\left(\frac{e^2}{4\pi\epsilon_0}\right)^2\right] \cdot \frac{1}{n^2}. \tag{2}$$

According to QM, light is emitted when the electron undergoes a transition from some initial state n_i to a lower-lying final state $n_f < n_i$. Using the relation $\Delta E = \frac{hc}{\lambda}$, it then follows that the emitted wavelength is

$$\frac{1}{\lambda} = \frac{\mu}{4\pi c\hbar^3}\left(\frac{e^2}{4\pi\epsilon_0}\right)^2\left(\frac{1}{n_f^2} - \frac{1}{n_i^2}\right), \tag{3}$$

thereby corroborating the empirical result in Eq. 1. Notably, the theoretical derivation shows that the Rydberg constant is proportional to μ. We will use this relationship to estimate the $^1\mathrm{H}/^2\mathrm{H}$ mass ratio based on the ratios of the Rydberg constants.

While Eq. 3 suggests that the spectral "lines" are delta functions in frequency, a more advanced treatment shows that the fundamental lineshape in frequency space is approximately Lorentzian. In addition, the thermal motion of the gas sample further broadens the spectral line through the Doppler effect. It can easily be shown that the latter results in a Gaussian broadening. With both effects, it is reasonable to expect the lineshape to be the convolution of Lorentzian and Gaussian functions, known to spectroscopists as the *Voigt profile*.[1] In our work, we find that the Voigt function is the best description of the lineshape, but that a Gaussian fit is sufficient to obtain the mean position of the spectral line.

2.2. Fine structure corrections

The eigenstates of the Coulombic field, corresponding to energies in Eq. 2, are n^2-fold degenerate. The degeneracy is broken when higher-order perturbations are considered. In particular, relativistic correction for the kinetic energy, and the magnetic coupling between the spin and orbital angular momenta of the electron yield splittings of the degenerate states of order $\alpha^2 E_1$. Called the fine structure corrections, the lifting of the degeneracy manifests itself spectroscopically by the *doublet structure* in the observed wavelengths, in which some emission lines are resolved to consist of two distinct peaks.

3. EXPERIMENTAL SETUP

We used the Jobin Yvon 1250M monochromator to diffract the various frequencies of the light from atomic discharge lamps. As shown in Fig. 1, the monochromator

featured a Czerny-Turner configuration with a selectable 1800gpmm or 3600gpmm grating. The instrument provided a mechanical counter associated with the orientation of the grating, which could be interpretated as a very coarse scale for the wavelength under analysis.

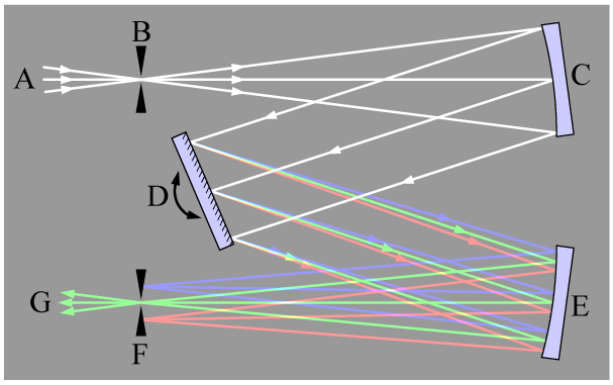

FIG. 1: The Czerny-Turner monochromator (Jobin Yvon 1250M). The central grating (1800gpmm or 3600gpmm) is under mechanical control, and can be rotated as to select a specific wavelength in the output plane. Image from [2]

The operational principles of the monochromator are as follows: The broadband light source (A) is placed in front of the monochromator input slit (B). In accordance with the Huygens principle, the input slit produces divergent waves in the apparatus. A spherical mirror (C) is then used to collimate the beam towards the grating (D) whose orientation is under mechanical control. A second spherical mirror (E) receives the first-order diffracted beams from the grating, and refocuses it on the output plane. By appropriately positioning the grating, different wavelengths are seleccted by the fixed output slit (F). Finally, a PMT at (G) collects the photon counts.

We have chosen to collect all data with the input and output slits set at 50 microns. The fundamental tradeoff between smaller and larger slit sizes is the competition between the quality of the lineshape and the size of the signal. For instance, if the light source is misaligned with respect to a large input slit, we expect (and observed) asymmetries in the resulting lineshape. In addition, when a large output slit is used, we are effectively convolving the underlying lineshape with a broad response function that smears away the resolution of the instrument. On the other hand, when the slit widths are too small, the signal disappears simply due to the lack of light.

Our choice of 50 microns slightly favors the signal size over the lineshape. This was acceptable since the degraded linewidths were still adequately fitted (Fig. 3), and also because the mean of the peak was still easily identifiable. The error in the fitted mean (at *any* slit configuration) is completely dominated by the shot-to-shot variation in setting the grating position, which is discussed next.

The scanning range was implemented by a precision stepping motor that would rotate the grating in the monochromator. Surprisingly, by scanning the same interval multiple times, we found that a single spectral line could be reported at various counter positions. This behavior is shown in Figure 2. We have seen similar variations in both 1800gpmm and 3600gpmm gratings, which implies that the error originates from the stepper motor.

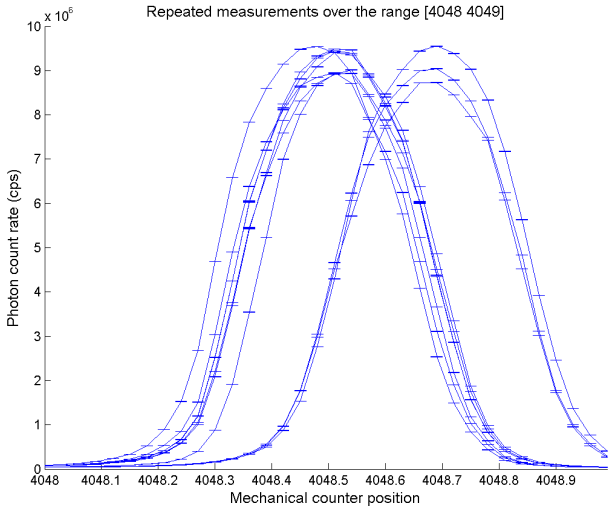

FIG. 2: Shot-to-shot variation in the location of a single spectral line. The peak is that of the 4046.56$\mathring{A}$ of mercury. With each run, the identical mechanical counter range of $[4048, 4049]$ was scanned.

As shown in Fig. 2, the shot-to-shot variation is not uniform, but rather appears to be bimodal. We have also observed that certain maneuvers can preferentially yield a particular mode, although our tests were not conclusive. Unfortunately, due to time constraints, most of our actual measurements were taken only once; hence we do not know which of the two modes we have observed with each measurement. Therefore, we have used 0.17$\mathring{A}$ (the separation between the means of the two modes) as the systematic error associated with every data point. This is consistent with the monochromator manual[3], which claims only 0.5$\mathring{A}$ accuracy in setting the motor position.

4. RESULTS AND DISCUSSION

4.1. Fitting the lineshape

The monochromator produces a photon detection rate vs. mechanical counter (i.e. grating orientation) curve as shown in Figure 3. The diagram also shows Voigt and Gaussian fits to the lineshape. Although the Voigt distribution is notably better ($\chi^2_{\nu-1} = 1.182$ vs. $\chi^2_{\nu-1} = 3.347$), both predict identical means. Due to the numerical ease of the Gaussian fit, we have chosen to compute all mean positions by using the latter. Typical errors in the fitting (0.001$\mathring{A}$) were completely negligible with respect to the 0.17$\mathring{A}$ mechanical error previously discussed.

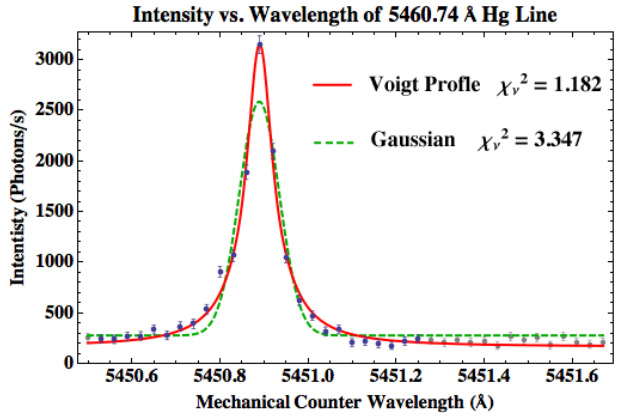

FIG. 3: The lineshape of the 5460.74$\AA$ Hg line under the 1800gpmm grating. Clearly, the Voigt profile is the better description. However, the two agree exactly in the mean position 5450.89, which is the final quantity we need to extract. Due to the numerical simplicity of the Gaussian fit, we have used the latter function in our analysis.

4.2. Mercury calibration

From the beginning, it was clear that the mechanical counter provided by the monochromator could not be used directly as an accurate indicator of wavelength. For example, in the 3600gpmm grating, there was a DC shift of approximately 80$\AA$ between the accepted wavelength of some spectral line, and the corresponding reading on the mechanical counter. Furthermore, we found that the deviation was nonlinear over the range of interest.

For both gratings, we have calibrated the mechanical counter scale by using all major lines in the mercury spectrum. By using the characteristic features of the Hg spectrum (for example, the doublet structure of 3131.55$\AA$ and 3131.84$\AA$) we were immediately able to establish a correspondence between the two scales. The result of this calibration for the 3600gpmm grating is in Table I.

TABLE I: Mercury calibration of the 3600gpmm grating. AW denotes "Accepted wavelength"; and MC denotes "Mechanical counter"

AW ($\AA$)	MC ($\AA$)	AW ($\AA$)	MC ($\AA$)
3125.67	3040.78	4046.56	3961.34
3131.55	3046.64	4077.83	3992.61
3131.84	3046.94	4339.22	4253.93
3650.15	3465.07	4358.33	4253.93
3662.88	3577.98	4916.07	4831.23
3663.28	3578.30		

From such Hg data, we produced a quadratic function to convert between physical wavelengths and the mechanical counter. The quadratic conversion function proved to be an excellent model, yielding $\chi^2_{\nu-1} = 0.97$. The function was then used to translate hydrogen, deuterium and sodium data into physical wavelengths. Interestingly, we have observed that the quadratic fit produced significant off-diagonal terms in the covariance matrix. Accordingly, we have found that it was crucial to use the full formula $\sigma_\lambda^2 = \sum_{i,j} cov(i,j) \cdot \partial_i\lambda \cdot \partial_j\lambda$ in propagating the errors.

4.3. Rydberg fits of hydrogen and deuterium

Our task in computing the Rydberg coefficient was greatly simplified by our knowledge that the observed spectra were the Balmer lines, characterized by $n_f = 2$. According to Eq. 1, it was also clear that longer wavelengths should be assigned smaller n_i, as in Table II. The measurement error incorporates the uncertainty in the conversion function parameters, in addition to the 0.17$\AA$ variation due to the grating positioning.

TABLE II: Observed wavelengths of $H = {}^1H$ and $D = {}^2H$ samples. All measurements have been converted to physical wavelengths by the Hg-based conversion formula. Results are given in angstroms.

n_i	λ_H	λ_D	$\Delta\lambda = \lambda_H - \lambda_D$
3^a	$6562.94 \pm .18$	$6561.60 \pm .18$	$1.34 \pm .26$
4	$4860.91 \pm .20$	$4859.83 \pm .21$	$1.08 \pm .29$
5	$4340.38 \pm .18$	$4339.17 \pm .18$	$1.21 \pm .26$
6	$4101.83 \pm .18$	$4100.73 \pm .18$	$1.11 \pm .26$
7	$3970.12 \pm .18$	$3969.07 \pm .18$	$1.04 \pm .26$
8	$3889.04 \pm .18$	$3888.05 \pm .18$	$0.99 \pm .26$
9	$3835.38 \pm .18$	$3834.54 \pm .20$	$0.83 \pm .26$

[a]The $n_i = 3$ line was outside of the scannable range of the 3600gpmm grating. It is the only data point for the ${}^1H/{}^2H$ experiment taken with the 1800gpmm grating.

We then plotted $1/\lambda$ as a function of n_i. Figure 4 shows the plot for hydrogen. Note that the $n_i = 3$ line was excluded since it was the only point taken with the low-density grating. For maximum consistency, we performed the ensuing analysis only for the lines with $n_i \geq 4$, which were all observed with the 3600gpmm grating. The plot was fitted with the Rydberg function (Eq. 1), producing $R_{H,ex} = (1.09711 \pm .00002) \times 10^7 \mathrm{m}^{-1}$. For a comparison to published values, we corrected for the index of refraction of air ($n = 1.0003$), which yielded $R'_{H,ex} = (1.09678 \pm .00002) \times 10^7 \mathrm{m}^{-1}$. This is in remarkable agreement with the NIST value[4] of $R_{NIST} = 1.096776 \times 10^7 \mathrm{m}^{-1}$. We applied the same analysis for the deuterium Rydberg: $R_{D,ex} = (1.09739 \pm .00002) \times 10^7 \mathrm{m}^{-1}$. (Index correction not applied.)

Given the ratio of the Rydbergs, it was then possible to compute the isotope mass ratio. Using the relation $R_H/R_D = \mu_H/\mu_D$ and the NIST values of m_e and m_p, we first computed m_D, from which the mass ratio could be obtained. This calculation yielded $m_D/m_H = 1.87 \pm 0.17$. The accepted value of $m_D/m_H = 1.999$ lies within our bounds. We can ascribe the large relative error on

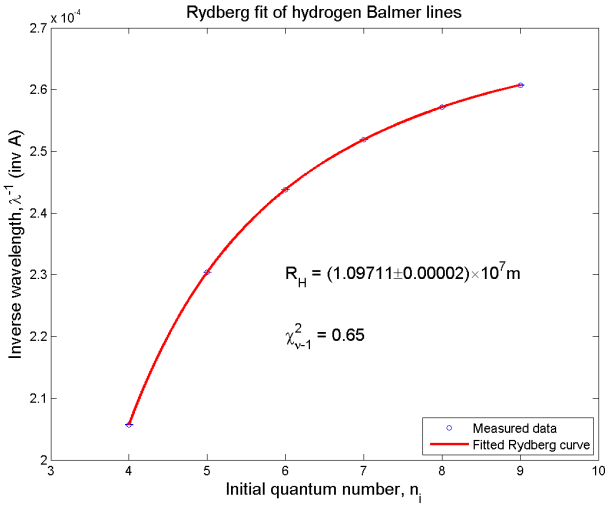

FIG. 4: Rydberg fit (Eq. 1) to the hydrogen Balmer lines.

the mass ratio, compared to the relative error on the Rydberg, to the functional relationship between the two quantities. In particular, recall that

$$\frac{1}{R} \propto \frac{1}{\mu} = \frac{1}{m_e} + \frac{1}{m_n} \tag{4}$$

where m_n is the mass of the nucleus. Since $m_n \gg m_e$, it can be seen that the nuclear mass has a very subdued effect on the overall reduced mass. It is therefore reasonable to expect large relative errors in m_n associated with minute relative errors in R.

4.4. Fine structure of sodium

In Table III we have tabulated eight pairs of doublet splittings in the sodium spectrum. The assignment of the corresponding atomic transition was aided by [5].

5. ERROR ANALYSIS

Clearly, the dominant limitation of our apparatus was the $0.17\mathring{A}$ error in the repeatability of the measurements. We suggest a more thorough testing of the monochromator in order to diagnose the behavior. (We have previously remarked that the behavior did not seem random.)

One technique to circumvent the motor positioning error is to superpose the calibration light on top of the sample. This could be done by the use of a beamsplitter. This would likely boost the precision of the apparatus to its stated resolving power ($R \approx 10^4 \rightarrow 0.03\mathring{A}$ precision), although this may not be possible at every wavelength. This will be a significant improvement expecially for the mass ratio measurement. The typical isotope shift for ^1H and ^2H is less than an angstrom; hence the pairs of lines can be taken in a single run. This would greatly improve upon the current $.26\mathring{A}$ error in $\Delta\lambda$.

TABLE III: The fine-structure splittings of sodium.

Transition	Accepted λ (Å)	Measured λ (Å)	Splitting (Å)
$4P_{3/2} \rightarrow 3S$	3302.37	3302.47 ± 0.18	0.69 ± 0.25
$4P_{1/2} \rightarrow 3S$	3302.98	3303.16 ± 0.18	
$7D \rightarrow 3P_{1/2}$	4494.18	4494.26 ± 0.19	3.48 ± 0.27
$7D \rightarrow 3P_{3/2}$	4497.66	4497.74 ± 0.18	
$6D \rightarrow 3P_{1/2}$	4664.81	4665.07 ± 0.18	3.74 ± 0.26
$6D \rightarrow 3P_{3/2}$	4668.56	4668.81 ± 0.18	
$7S \rightarrow 3P_{1/2}$	4747.94	4747.47 ± 0.20	3.94 ± 0.28
$7S \rightarrow 3P_{3/2}$	4751.82	4751.42 ± 0.19	
$5D \rightarrow 3P_{1/2}$	4978.54	4978.38 ± 0.18	4.41 ± 0.26
$5D \rightarrow 3P_{3/2}$	4982.81	4982.79 ± 0.18	
$4D \rightarrow 3P_{1/2}$	5682.63	5682.36 ± 0.18	5.70 ± 0.26
$4D \rightarrow 3P_{3/2}$	5688.21	5688.05 ± 0.18	
$3P_{3/2} \rightarrow 3S$	5889.95	5890.04 ± 0.18	5.89 ± 0.26
$3P_{1/2} \rightarrow 3S$	5895.92	5895.94 ± 0.18	
$5S \rightarrow 3P_{1/2}$	6154.23	6152.67 ± 0.63	4.96 ± 0.89
$5S \rightarrow 3P_{3/2}$	6160.75	6157.63 ± 0.63	

6. CONCLUSIONS

We have performed spectroscopy on hydrogen, deuterium and sodium. The basic Rydberg formula was verified for hydrogen and deuterium ($\chi^2_{\nu-1} = 0.65, 0.43$ respectively). Our measured value of the hydrogen Rydberg constant agrees with the NIST value extremely well: $R'_{H,ex} = (1.09678 \pm .00002) \times 10^7 \mathrm{m}^{-1}$ vs. $R_{NIST} = 1.096776 \times 10^7 \mathrm{m}^{-1}$. We have also estimated the mass ratio of the isotopes, and found $(m_D/m_H)_{ex} = 1.87 \pm 0.17$, which contains the expected $(m_D/m_H)_{NIST} = 1.999$. Finally, we suggested an improvement to the optical setup, that can notably improve the estimate of the mass ratio.

[1] H. Kuhn, *Atomic Spectra* (Academic Press, 1969).
[2] http://en.wikipedia.org/wiki/Monochromator.
[3] S. Industries, *M-series spectrometers.*
[4] NIST, *1998 codata recommended values of the fundamental constants of physics and chemistry.*
[5] A. Melissinos, *Experiments in Modern Physics* (Academic Press, 1966).

Acknowledgments

THK gratefully acknowledges Connor McEntee for his partnership in the experiment. THK also thanks the Junior Lab staff for statistical guidance, and the suggestion of the index of refraction correction.